Tailoring UV cure depth profiles for optimal mechanical properties of organosilicate thin films

Taek-Soo Kim,[1] Dmytro Chumakov,[2] Ehrenfried Zschech,[2] and Reinhold H. Dauskardt[3,a)]
[1]*Department of Mechanical Engineering, Stanford University, Stanford, California 94305, USA*
[2]*Globalfoundries Dresden Module One LLC and Co. KG, Wilschdorfer Landstrasse 101, Dresden, Saxony 01109, Germany*
[3]*Department of Materials Science and Engineering, Stanford University, Stanford, California 94305, USA*

(Received 20 June 2009; accepted 5 July 2009; published online 18 August 2009)

The adhesive and cohesive properties of organosilicate thin films are remarkably insensitive to UV curing. We demonstrate how to maximize these properties with UV standing waves together with an optical spacer underlying layer. Using a simulation of the UV cure profile through the film thickness, we demonstrate how a UV transparent SiN optical spacer layer can be selected to maximize curing at both sides of the organosilicate film with marked increases in interfacial fracture energy. On the contrary, a UV absorbing SiCN underlying layer resulted in significantly reduced UV intensities and small improvements of the interfacial fracture energies. © *2009 American Institute of Physics*. [DOI: 10.1063/1.3190198]

Organosilicate thin film glasses (OSGs) have applications as low dielectric constant (k) materials in microelectronic interconnect layers,[1] selective membranes,[2] biosensors,[3] optical waveguides,[4] and antireflective coatings.[5] However, their mechanically fragile nature and susceptibility to environment-assisted cracking have made integration into complex device structures challenging.[6–8,10–13] Significant efforts have been directed to improving their mechanical properties by postdeposition treatments such as thermal,[14] plasma,[15] e-beam,[14] and UV curing.[9–14] UV curing has been demonstrated to significantly increase the elastic modulus, hardness, and fracture energy while inducing relatively minor increase in dielectric properties.[9–14,16] However, the adhesive fracture energy at the bottom interface and the cohesion in the middle of the OSG film are remarkably insensitive to UV curing compared to adhesion at the top interface.[9–12]

While the bottom interface is sometimes weaker due to a higher carbon content near the bottom interface (<10 nm) resulting from partially dissociated precursors during a typical plasma enhanced chemical vapor deposition (PECVD),[17] the UV curing is nevertheless ineffective in improving the adhesion at the bottom interface. We previously demonstrated the insensitivity of the fracture energy at the bottom to UV curing is related to depth dependent UV curing through the OSG film thickness by the UV standing wave effect.[9,10] It was shown that UV light intensity at the bottom interface of the OSG on a highly reflecting underlying layer has a minimum value due to destructive light interference, which leads to the relatively small increase in the fracture energy at the bottom by the UV curing. The nonuniform curing that results through the film thickness was apparent by observing a corresponding change in the elastic stiffness of the film.[9,10]

In the present study, we demonstrate how to maximize the UV light intensity and therefore the fracture energy at both top and bottom interfaces of the OSG film by exploiting the UV standing wave effect and an underlying barrier layer as an optical spacer. The model predicts the UV cure intensity, U, as a function of film depth, z, and cure duration, t,[10]

$$U(z,t) = \int_0^t I_2[h(t),n(t),z]dt, \quad (1)$$

where I_2 is the standing wave intensity in an OSG film on a Si substrate, which can be obtained by squaring the magnitude of the electric field of the standing waves within the film, ε_2. We initially extend our UV curing model to account for multilayer films by considering an OSG film on an underlying UV transparent barrier [Fig. 1(a)]. An electric field of a standing wave within the OSG film [region (2)] can be analytically expressed as

$$\varepsilon_2(z) = \varepsilon_I \tau_{12} \frac{\exp(-ik_2 z) + \rho'_{23}\tau^2_{h_2}\exp(ik_2 z)}{1 + \rho_{12}\rho'_{23}\tau^2_{h_2}}, \quad (2)$$

where

$$\rho'_{23} = \frac{\boldsymbol{n}_2 - \boldsymbol{n}_3 X_3}{\boldsymbol{n}_2 + \boldsymbol{n}_3 X_3}, \quad X_3 = \frac{1 - \rho_{34}\tau^2_{h_3}}{1 + \rho_{34}\tau^2_{h_3}}, \quad (3)$$

and ε_I is the incident wave at $z=0$, $\rho_{ij}=(n_i-n_j)/(n_i+n_j)$ is the reflection coefficient, $\tau_{ij}=2n_i/(n_i+n_j)$ is the transmission coefficient, $\tau_{hj}=\exp(-ik_j h_j)$ is the internal transmittance of the thin film, $k_j=2\pi n_j/\lambda$ is the propagation constant, $\boldsymbol{n}_j=n_j-i\kappa_j$ is the complex index of refraction, n_j is the refractive index, and κ_j is the extinction coefficient.[18] Indices refer to layers as defined in Fig. 1(a). By incorporating Eq. (2) into

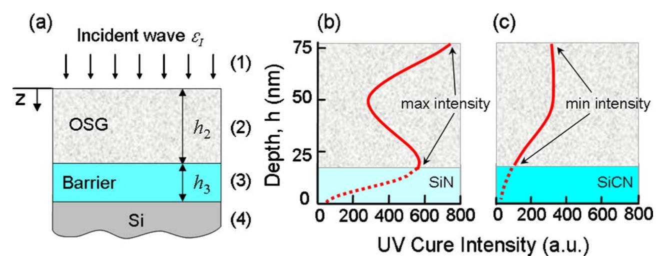

FIG. 1. (Color online) (a) Film stack showing geometry for the derivation of an extended UV curing depth profile model. UV cure intensity depth profiles through the OSG film on (b) UV transparent and (c) UV absorbing underlying layers, respectively.

a)Electronic mail: dauskardt@stanford.edu.

0003-6951/2009/95(7)/071902/3/$25.00

© 2009 American Institute of Physics

Downloaded 19 Aug 2009 to 128.12.153.62. Redistribution subject to AIP license or copyright; see http://apl.aip.org/apl/copyright.jsp

our UV cure depth profile model described by Eq. (1), the effect of the underlying optical spacer layer on the resulting UV cure depth profile can be explicitly predicted.

Through optimization of the thickness and optical properties of the underlying layer using the extended model, maximum UV cure intensities at both the top and bottom interfaces of the OSG layer can be achieved. Using a UV curing wavelength of 172 nm and the refractive index and absorption properties of the OSG and barrier layer, it was found that a 20 nm thick UV transparent SiN underlying layer (absorption coefficient, $\alpha < 7 \times 10^3$ cm^{-1}) results in maximum UV cure intensities at both the top and bottom interfaces of the OSG, whereas a typical UV absorbing SiCN layer ($\alpha > 3 \times 10^5$ cm^{-1}) resulted in minimum intensities as shown in Figs. 1(b) and 1(c), respectively. The presence of a zero standing wave intensity that leads to no curing is apparent at the interface with Si. The 20 nm thickness was selected to avoid this zero intensity and locate a maximum intensity at the bottom of the OSG film, utilizing the underlying layer as an optical spacer [Fig. 1(b)].

OSG films with dielectric constant $k \sim 2.6$ and thickness ranging from 65 to 180 nm were deposited by PECVD on blank Si substrates, and on 20 nm thick SiN and SiCN underlying layers, respectively. The underlying layers were also deposited by PECVD on Si substrates. After deposition, they were exposed to monochromatic UV radiation with wavelength $\lambda = 172$ nm for 5 min in a controlled environment. Following the UV cure, the films were capped with PECVD SiCN barrier layers. The force modulation atomic force microscopy (FM-AFM) technique[9,10] was used to investigate the variations in the elastic modulus on the cross-section of specimens containing the UV cured organosilicate films. Two thin film structures were bonded with epoxy, and the specimen consisting of the two thin film structures were diced and polished by chemical mechanical planarization to produce a flat cross-section. The AFM tip always remained in contact with the surface during force modulation scans on the cross-section. The elastic modulus was quantified using Hertzian contact mechanics to consider the deformation of both the surface and the tip. Time-of-flight secondary ion mass spectrometry (TOF-SIMS) was used for the depth profiling of chemical compositions through the films. Four-point bend and double cantilever beam specimen geometries were fabricated and tested to measure adhesive and cohesive fracture energies of the OSG films, respectively.[9,10,19,20] After testing, the specimens were examined using high resolution x-ray photoelectron spectroscopy to determine the fracture path in the thin-film structures.

A force modulation signal image of a cross-section of a specimen containing an initially 180 nm thick UV cured OSG film on a Si substrate is shown in Fig. 2(a). The force modulation signal was converted to elastic modulus, E, using Hertzian contact mechanics and the elastic modulus depth profile [a black line in Fig. 2(b)] had only one peak in the middle with very severe undulation and the profile is consistent with a prediction [a red line in Fig. 2(b)] simulated using the UV standing wave model. The discrepancy between the measured and predicted elastic modulus becomes larger toward both interfaces. The measured elastic modulus of the OSG near the interfaces was overestimated due to the AFM tip beginning to sample the stiff adjacent Si and SiCN materials ($E > 160$ GPa). Such tip convolution limits the spatial

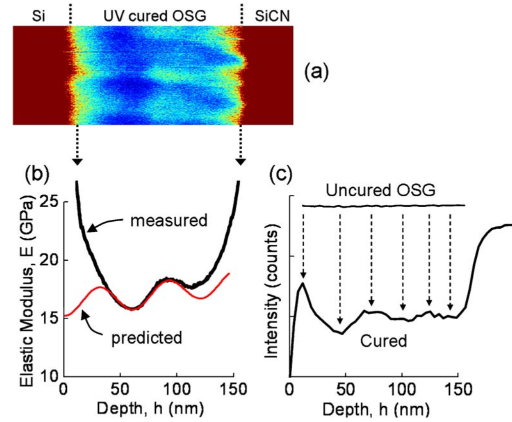

FIG. 2. (Color online) (a) A force modulation signal image of a cross-section of a specimen containing a UV cured OSG film, (b) an elastic modulus depth profile of the OSG film measured by FM-AFM (black line) is compared with predicted one by the standing wave simulation (red line), and (c) TOF-SIMS depth profiling for the carbon content through the OSG films before and after UV curing.

resolution of the FM-AFM technique near the interfaces.

TOF-SIMS depth profiling for carbon content was performed through the OSG films before and after the UV curing [Fig. 2(c)] to demonstrate that the UV cure intensity at the bottom of the UV cured OSG was a minimum by destructive light interference on a highly reflecting Si substrate. Depletion of carbon content is an indication of UV curing reactions involving loss of terminal methyl groups and subsequent formation of glass backbone bonds.[11,13,16] A horizontal line in Fig. 2(c) represents a depth profile for the carbon content of the uncured OSG film. Following the UV cure, significant decrease in the carbon content was observed and the depth profile was not uniform. The carbon content oscillated with the same periodicity as that of predicted elastic modulus depth profile shown in Fig. 2(b). However, the most interesting finding was a carbon peak at the bottom interface, which means that the bottom underwent the minimum UV cure intensity as predicted. This suggests the possibility of increasing the fracture energy at the bottom of the layer by increasing the UV cure intensity using the optical spacer layer discussed above.

A UV transparent SiN layer was used for the underlying optical spacer layer and compared to a UV absorbing SiCN layer. We note that they are currently used as barrier layers to Cu diffusion. The SiCN film can significantly absorb high energy UV light depending on its carbon content.[21,22] It was expected that the UV transparent SiN would work as an optical spacer to relocate the UV intensity maximum at the bottom interface of the OSG film. Figure 3 shows the simulated UV cure intensity depth profiles in a 65 nm thick OSG film deposited on SiCN and SiN, respectively, and their measured fracture energies. As shown in the simulated UV cure intensity depth profile for the OSG on SiCN [Fig. 3(a)], UV cure intensity at the bottom is very small because of strong UV light absorption by the SiCN underlying layer. Consequently fracture energy at the bottom was not improved by the UV curing, although fracture energy at the top increased noticeably [Fig. 3(b)]. On the contrary, the UV transparent SiN underlying layer had totally different results. The simulated UV cure intensity depth profile shows maximum UV cure intensities both at the top and bottom [Fig. 3(c)]. The measured fracture energy was dramatically increased not

Downloaded 19 Aug 2009 to 128.12.153.62. Redistribution subject to AIP license or copyright; see http://apl.aip.org/apl/copyright.jsp

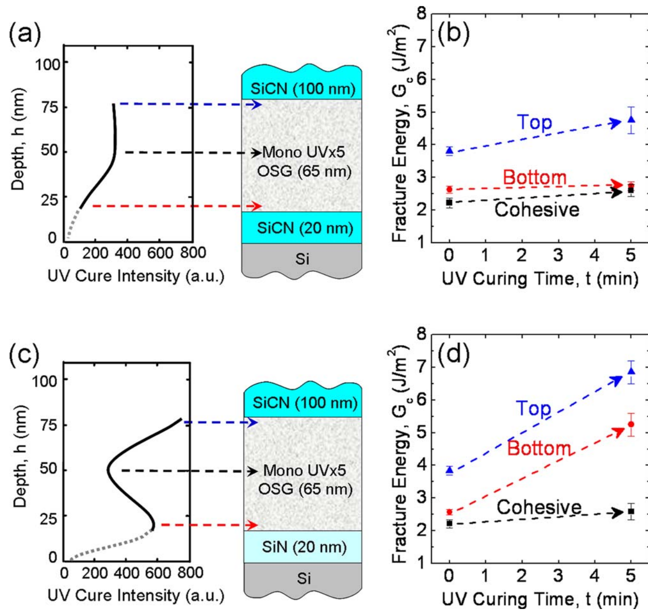

FIG. 3. (Color online) Simulated UV cure intensity depth profiles in 65 nm thick OSG films deposited on (a) SiCN and (c) SiN, and measured fracture energies for the OSG films on (b) SiCN and (d) SiN, respectively.

only at the top but also at the bottom [Fig. 3(d)]. The fracture energy at the bottom increased by almost 100% from 2.6 to 5.3 J/m^2 following the UV curing. The same trend was observed for the thicker OSG film as shown in Fig. 4, however, with somewhat less increase of the fracture energies at the top and bottom of the 100 nm thick OSG film on SiN due to increased absorbance of the thicker OSG film.

The results clearly demonstrate that significant enhancement in fracture energies at both interfaces of OSG films can be obtained by tailoring the UV curing depth profiles and employing the underlying barrier as an optical spacer. Minimum UV curing at the bottom of an OSG film on a reflecting Si substrate was confirmed with TOF-SIMS depth profiling. A 20 nm thick UV transparent SiN underlying layer was

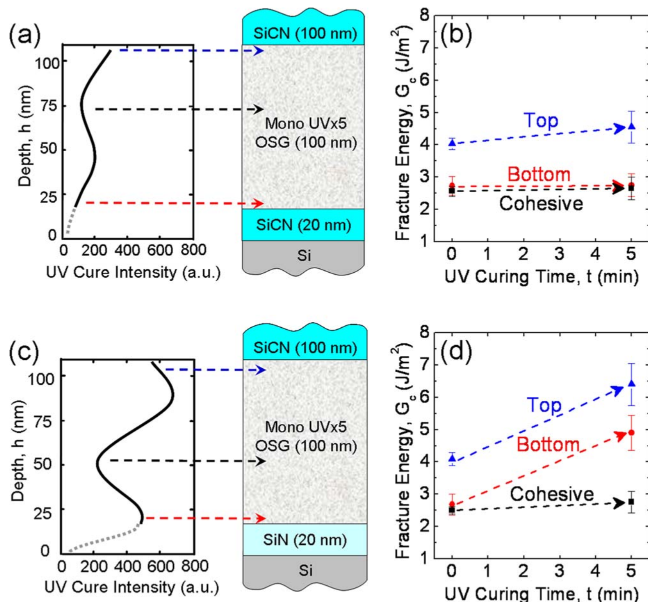

FIG. 4. (Color online) Simulated UV cure intensity depth profiles in 100 nm thick OSG films deposited on (a) SiCN and (c) SiN, and measured fracture energies for the OSG films on (b) SiCN and (d) SiN, respectively.

shown to work as an optical spacer to locate maximum UV intensities at both interfaces of the OSG film resulting in dramatic increases in the interfacial fracture energies. On the contrary, a UV absorbing SiCN underlying layer resulted in significantly reduced UV intensities and small improvements of the fracture energies at the interfaces because of strong UV light absorption.

We note finally that the implications of this study are not limited to OSG films, but have broader applications for thin film technologies employing UV curing. A promising further application of this study is the possibility of fabricating films with graded mechanical and physical properties with a single post deposition UV curing process. For example, dielectric films could be made with high elastic modulus and fracture resistance at the top, preservation of ultralow k value in the middle, and high adhesion and ash tolerance at the bottom, as is desired for next generation microelectronic interconnects.[23]

This work was supported by the Director, Office of Energy Research, Office of Basic Energy Sciences, Materials Sciences Division of the U.S. Department of Energy, under Contract No. DE-FG02-07ER46391.

[1]A. Grill *et al.*, *Proceedings of the IEEE International Interconnect Technology Conference* (IEEE, Piscataway, NJ, 2008), p. 28.
[2]A. K. Cheetham, G. Ferey, and T. Loiseau, Angew. Chem., Int. Ed. **38**, 3268 (1999).
[3]T. A. Desai, D. J. Hansford, L. Leoni, M. Essenpreis, and M. Ferrari, Biosens. Bioelectron. **15**, 453 (2000).
[4]W.-C. Chen, L.-H. Lee, B.-F. Chen, and C.-T. Yen, J. Mater. Chem. **12**, 3644 (2002).
[5]S. Kim, J. Cho, and K. Char, Langmuir **23**, 6737 (2007).
[6]E. P. Guyer and R. H. Dauskardt, Nature Mater. **3**, 53 (2004).
[7]E. P. Guyer and R. H. Dauskardt, J. Mater. Res. **20**, 680 (2005).
[8]E. P. Guyer, M. Patz, and R. H. Dauskardt, J. Mater. Res. **21**, 882 (2006).
[9]T. Kim, N. Tsuji, N. Kemeling, K. Matsushita, D. Chumakov, H. Geisler, E. Zschech, and R. H. Dauskardt, J. Appl. Phys. **103**, 064108 (2008).
[10]T. Kim, N. Tsuji, K. Matsushita, N. Kobayashi, D. Chumakov, H. Geisler, E. Zschech, and R. H. Dauskardt, J. Appl. Phys. **104**, 074113 (2008).
[11]D. M. Gage, J. F. Stebbins, L. Peng, Z. Cui, A. Al-Bayati, K. P. MacWilliams, H. M'Saad, and R. H. Dauskardt, J. Appl. Phys. **104**, 043513 (2008).
[12]Y. Lin, Y. Xiang, T. Y. Tsui, and J. J. Vlassak, Acta Mater. **56**, 4932 (2008).
[13]F. Iacopi, Y. Travaly, B. Eyckens, C. Waldfried, T. Abell, E. P. Guyer, D. M. Gage, R. H. Dauskardt, T. Sajavaara, K. Houthoofd, P. Grobet, P. Jacobs, and K. Maex, J. Appl. Phys. **99**, 053511 (2006).
[14]D. M. Gage, K. S. Yim, A. Al-Bayati, A. Demos, H. M'Saad, and R. H. Dauskardt, *Proceedings of Advanced Metallization Conference* (Materials Research Society, Warrendale, PA, 2008), p. 433.
[15]H. Namatsu and K. Minegishi, J. Electrochem. Soc. **140**, 1121 (1993).
[16]F. Iacopi, G. Beyer, Y. Travaly, C. Waldfried, D. M. Gage, R. H. Dauskardt, K. Houthoofd, P. Jacobs, P. Adriaensens, K. Schulze, S. E. Schulz, S. List, and G. Carlotti, Acta Mater. **55**, 1407 (2007).
[17]A. Grill, D. Edelstein, M. Lane, V. Patel, S. Gates, D. Restaino, and S. Molis, J. Appl. Phys. **103**, 054104 (2008).
[18]C. A. Mack, Appl. Opt. **25**, 1958 (1986).
[19]R. H. Dauskardt, M. Lane, Q. Ma, and N. Krishna, Eng. Fract. Mech. **61**, 141 (1998).
[20]R. J. Hohlfelder, D. A. Maidenberg, R. H. Dauskardt, Y. Wei, and J. W. Hutchinson, J. Mater. Res. **16**, 243 (2001).
[21]C. W. Chen, C. C. Haung, Y. Y. Lin, L. C. Chen, K. H. Chen, and W. F. Su, Diamond Relat. Mater. **14**, 1010 (2005).
[22]C. W. Chen, C. C. Haung, Y. Y. Lin, W. F. Su, L. C. Chen, and K. H. Chen, Appl. Phys. Lett. **88**, 073515 (2006).
[23]M. Tada, H. Yamamoto, F. Ito, M. Narihiro, M. Ueki, N. Inoue, M. Abe, S. Saito, T. Takeuchi, N. Furutake, T. Onodera, J. Kawahara, K. Arai, Y. Kasama, T. Taiji, M. Tohara, M. Sekine, and Y. Hayashi, Tech. Dig. - Int. Electron Devices Meet. **2006**, 346781.

Downloaded 19 Aug 2009 to 128.12.153.62. Redistribution subject to AIP license or copyright; see http://apl.aip.org/apl/copyright.jsp